THE AMERICAN SOCIETY OF MECHANICAL ENGINEERS
345 E. 47 St., New York, N.Y. 10017

83-GT-28

HEAT TRANSFER CHARACTERISTICS FOR JET ARRAY IMPINGEMENT WITH INITIAL CROSSFLOW

L.W. Florschuetz
Member,
ASME

D.E. Metzger
Member,
ASME

C.C. Su
Student Member,
ASME

Department of Mechanical and Aerospace Engineering
Arizona State University
Tempe, Arizona 85287

ABSTRACT

Two-dimensional arrays of circular air jets impinging on a heat transfer surface parallel to the jet orifice plate are considered. The jet flow, after impingement, is constrained to exit in a single direction along the channel formed by the jet orifice plate and the heat transfer surface. In addition to the crossflow which originates from the jets following impingement, an initial crossflow is present which approaches the array through an upstream extension of the channel. The temperature of the initial crossflow air may differ from the jet air temperature. The configurations considered are intended to model the impingement cooled midchord region of gas turbine airfoils in cases where an initial crossflow is also present. Nusselt numbers and dimensionless adiabatic wall temperatures resolved to one streamwise jet hole spacing were experimentally determined for ratios of the initial crossflow rate to the total jet flow rate ranging from zero to unity. These are presented and discussed relative to the flow and geometric parameters.

NOMENCLATURE

A_o = total jet hole area
A_o^* = ratio of jet hole area to opposing impingement surface area (open area ratio), $\pi/[4(x_n/d)(y_n/d)]$
b = local thickness of jet plate at jet hole location
C_D = jet plate discharge coefficient
c_p = constant pressure specific heat
d = jet hole diameter
D_h = hydraulic diameter
f = friction coefficient defined as $2\tau_w\rho/G_c^2$
G_c = crossflow mass velocity based on channel cross-sectional area
G_j = jet mass velocity based on jet hole area
h = heat transfer coefficient at impingement surface defined by Eq. (1)
L = streamwise length of jet plate and impingement surface (Fig. 3)
L_e = initial crossflow development (entrance) length upstream of jet array
m_c = initial crossflow rate
m_j = total jet flow rate
N_c = number of spanwise rows of holes in streamwise direction
N_s = number of jet holes across span of heat transfer test surface
N_s' = number of jet holes across span of channel
Nu = Nusselt number, hd/k
q = heat flux at impingement surface
Q_n = heat rate at surface of test plate segment n in initial crossflow channel
Re_c = crossflow (channel) Reynolds number, $G_c(2z)/\mu$
Re_j = jet Reynolds number, $G_j d/\mu$
T_{aw} = adiabatic wall temperature
T_c = characteristic temperature of initial crossflow
T_j = characteristic temperature of jet flow
T_f = characteristic injection temperature for film cooling
T_m = characteristic mainstream temperature for film cooling
T_o^c = initial crossflow plenum air temperature
T_s = heat transfer surface temperature
w = width (span) of channel
x = streamwise location along jet plate or impingement surface (Fig. 3)
x_n = streamwise jet hole spacing
y_n = spanwise jet hole spacing
z = channel height (jet exit plane-to-impingement surface spacing)

Greek

η = dimensionless adiabatic wall temperature defined by Eq. (3) for jet array impingement with initial crossflow; and by Eq. (2) for film cooling.
μ = dynamic viscosity
ρ = fluid density
τ_w = channel wall shear stress

Superscript

$(\overline{\ })$ = overbar refers to mean value over jet plate

INTRODUCTION

Modern high performance engines use 20 percent or more of the compressor discharge flow for cooling purposes. The design of such engines requires great care so that the performance improvement to be derived from operating at higher temperatures is not more than offset by the cycle and aerodynamic penalties associated with compressing and using the cooling air. In order to do rational and confident design, the designer must have access to detailed accurate information on the flow and heat transfer characteristics of cooling schemes in use or under consideration.

The most critical areas in the engine from the viewpoint of thermal exposure are the first-stage airfoils, both stator vanes and turbine blades. The stationary first stage vanes, situated immediately downstream of the burner experience the highest gas temperatures, including ''hot streaks'' of several hundred degrees above the mean temperature associated with combustor pattern nonuniformities. The first stage blades, although experiencing lower relative velocities and a rotational averaging of the combustor pattern, are subject to the additional complications and stresses of rotation.

The large external heat loads require an internal cooling scheme with high heat transfer coefficients between the cooling air and inner surface of the airfoil. An impingement cooled arrangement is often the choice because of the high heat transfer coefficients possible and the capability of placing jets in patterns dictated by the external thermal loading. This flexibility in jet placement can be advantageous not only in the chordwise direction, but also in the spanwise direction to reflect, for example, the burner pattern in the radial direction. Fig. 1 shows a typical midspan arrangement of jets. Note that the jets are constrained to exit in the chordwise direction; so the accumulated jet flow from upstream rows acts as a crossflow to downstream jet rows in the array. The drop-off in external load behind the leading edge eliminates the need for new cooling jets in this region and the leading edge coolant flows around to become a separate, or initial, crossflow to the midchord jet array. Alternate types of arrangements, for example Fig. 2, do not include the presence of an initial crossflow approaching the midchord jet array.

Over the past several years, Arizona State University has engaged in a NASA sponsored study of the flow and heat transfer characteristics of two-dimensional jet arrays of the type depicted in the midchord regions of Figs. 1 and 2. The early work in this study was directed at modeling uniform arrays in cases where an initial crossflow is not present [1,2]. It should be recognized, however, that crossflow is always present downstream of the first row, whether or not a separate initial crossflow is imposed. The geometry of the airfoil application dictates that all of the jet flow will exit in the chordwise direction toward the trailing edge. This fact has stimulated much of the prior work on the effects of crossflow on confined jets, as typified by [1-11].

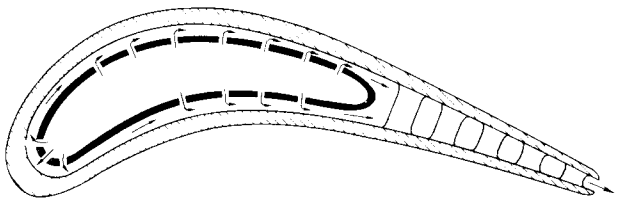

Fig. 1 Impingement cooled airfoil - midchord jet arrays subject to initial crossflow.

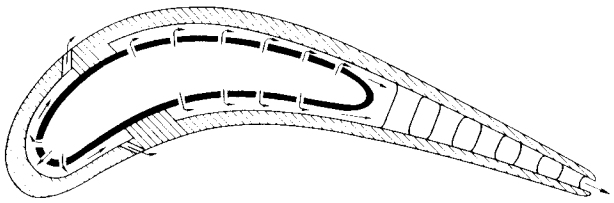

Fig. 2 Impingement cooled airfoil - midchord jet arrays not subject to initial crossflow.

More recently, the NASA sponsored study was expanded to consider the effects of initial crossflow, including the effect an initial crossflow temperature which is elevated above the jet temperature. The latter condition is of considerable importance. The designer is often faced with an initial crossflow temperature which is substantially above the jet flow because of heat pickup in the leading edge region. Confident design can be achieved only if the designer knows the proper effective coolant temperatures and heat transfer coefficients to use in the region where the initial crossflow penetrates into the jet array. To date, there appears to be little or no information in the literature to help the designer answer these questions.

This paper reports some results of the present study intended to respond to this need. Heat transfer coefficients and adiabatic wall temperatures resolved to one streamwise hole spacing were experimentally determined for uniform rectangular arrays of circular jet orifices with initial crossflow. The arrays are intended to model the types of midchord cooling arrangements illustrated schematically in Fig. 1. Streamwise and spanwise hole spacings, expressed in jet hole diameters (x_n/d, y_n/d) were (5,4), (5,8), (10,4) and (10,8). Each array had ten spanwise rows of holes. The jet plate-to-impingement surface spacings (z/d) were 1, 2, and 3 hole diameters. The configuration with (x_n/d, y_n/d, z/d) = (5,4,3) was also tested in a staggered hole pattern. Most tests were conducted with a nominal mean jet Reynolds number $\overline{Re}_j$ of 10^4. The ratio of initial crossflow rate to total jet flow rate (m_c/m_j) was set at nominal values of 0.2, 0.5, and 1.0 for each geometry with a reference test at zero initial crossflow also included. Both Nusselt numbers and dimensionless adiabatic wall temperatures are presented and discussed in relation to the flow and geometric parameters. Flow distribution effects associated with the presence of an initial crossflow were previously reported in detail in [12].

INITIAL CROSSFLOW EXPERIMENTAL FACILITY

The basic test model geometry and nomenclature are shown schematically in Fig. 3. The flow region of primary interest is that bounded by the jet exit plane and the impingement surface. The length (L) of this region is considered to extend from one-half a streamwise hole spacing ($x_n/2$) upstream of the first spanwise row of holes to the same distance downstream of the last row. The total crossflow rate approaching a given row is equivalent to the initial crossflow rate (m_c) combined

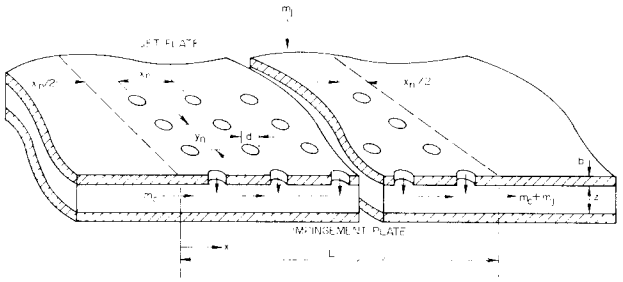

Fig. 3 Initial crossflow basic test model geometry and nomenclature.

with the total jet flow introduced upstream of that row.

The basic experimental facility was that originally used for a comprehensive series of noninitial crossflow tests [1,2], but set up in a modified form suitable for conducting tests with initial crossflow. A complete description of the original facility may be found in [1]. Here a description of the facility in the initial crossflow configuration will be given. For the convenience of the reader certain basic features previously described in detail [1], will also be noted.

A cross-sectional view of the arrangement is shown in Fig. 4. There are two plenum chambers, each with two sections of porous plenum packing supported by screens, supplied individually with dried and filtered laboratory compressed air, one for introducing air to the main jet plate, and one for introducing the initial crossflow air to the channel. An electric resistance heater (not shown) in the line immediately upstream of the initial crossflow plenum permits independent control of the initial crossflow air temperature at levels above the jet plenum air temperatures. The initial crossflow was introduced to the channel through two spanwise rows of jet holes. The main jet plates, each with ten spanwise rows of holes, are interchangeable. The plenum/jet plate assembly was mounted over the test plate unit (impingement plate) through interchangeable spacers which fixed the channel height (i.e., the jet exit plane-to-impingement surface spacing). The spacers also formed the upstream end-surface and side

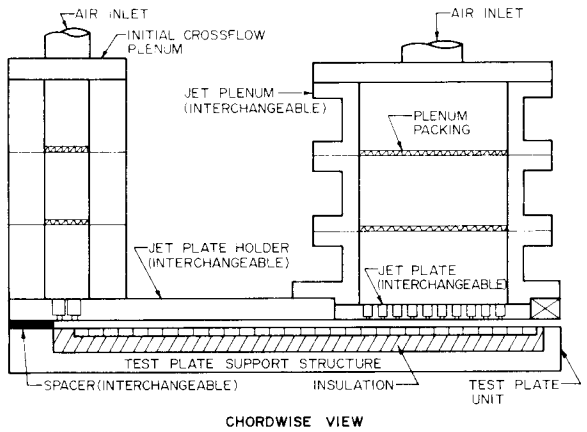

Fig. 4 Initial crossflow test facility schematic.

walls of the channel, thus constraining the initial crossflow and the jet flow to discharge in a single direction to the laboratory environment at atmospheric pressure. The test plate unit consists of a segmented copper heat transfer test plate with individual segment heaters, the necessary thermal insulation, and the test plate support structure. The segmented design provides for control of the streamwise thermal boundary condition at the heat transfer surface, as well as for determination of spatially resolved heat transfer coefficients in the streamwise direction. Note that in the configuration shown the spanwise rows of jet holes are centered over the test plate segments, one row per segment. This results in a streamwise resolution of measured heat transfer coefficients equivalent to one streamwise jet hole spacing. There are a total of 31 segments in the test plate, 19 upstream of the jet array, 10 immediately opposite the array, and two downstream of the array.

Significant geometric characteristics of the configurations tested are summarized in Table 1. The

Table 1. Geometric Parameters and Mean Discharge Coefficients for Jet Plates Tested.

Jet Plate $B(x_n/d, y_n/d)I$	A_o^*	d and b (cm)	N_s	N_s'	$\bar{C}_D$
B(5,4)I(&S)	0.0393	0.254	12	18	0.85
B(5,8)I	0.0196	0.254	6	9	0.80
B(10,4)I	0.0196	0.127	24	36	0.76
B(10,8)I	0.0098	0.127	12	18	0.76

Channel heights, (z/d) = 1, 2, and 3

Fixed Parameters:
Channel width (span), w = 18.3 cm
Heat transfer test plate width, 12.2 cm
Heat transfer test plate length, 39.4 cm
Overall channel length, 43.2 cm
Initial crossflow channel length, 26.0 cm
B-size jet array and plenum length, L = 12.7 cm
Downstream exit length, 4.5 cm
Initial crossflow development length, 24.1 cm
Number of spanwise rows of jet holes, N_c = 10
I = Inline, S = staggered hole pattern

array of length L = 12.7 cm with matching jet plenum (Fig. 4) was designated as size B. The jet plates are identified by the notation $B(x_n/d, y_n/d)I$ where the I designates an inline hole pattern, replaced by S to designate a staggered pattern. A staggered pattern was identical to its inline counterpart, except that alternating spanwise rows of holes were offset by one-half the spanwise spacing. Note that the overall channel width exceeded the width of the heat transfer test plate and that the number of holes across the channel (N_s') exceeded the number across the test plate (N_s). Jet holes were always symmetrically aligned with both the edges of the channel and the edges of the heat transfer test plate. Reckoned from the centerline of the second (i.e., downstream) spanwise jet row of the initial crossflow plenum, the channel length available for flow development upstream of the jet array (initial crossflow development length, 24.1 cm) ranged from 16 to 95 hydraulic diameters, depending on the channel height. It may also be noted that this length was 19 times the streamwise hole spacing in the main jet array (x_n = 1.27 cm). Average jet plate discharge coefficients are also included in Table 1.

IMPINGEMENT WITH CROSSFLOW AS A THREE-TEMPERATURE PROBLEM

The simplest and most frequently encountered convection heat transfer conditions can usually be treated in terms of two characteristic temperatures - a surface temperature and a fluid temperature (a two-temperature problem). Jet array impingement cooling with initial crossflow (Fig. 3) in which the initial crossflow temperature differs from that of the jets can be viewed as a three-temperature problem. This is a convection heat transfer situation where the surface heat transfer is to a fluid in the process of mixing from two different sources at two different temperatures. The best known example of a three-temperature situation is film cooling. In film cooling it is well known that the interaction of a secondary fluid stream with a primary stream affects not only the heat transfer coefficient, but also the value of the reference fluid temperature which drives the heat flux. In the simplest terms (Fig. 5):

$$q = h\,(T_s - T_{aw}) \tag{1}$$

where T_{aw} is the adiabatic wall temperature and is embodied in a non-dimensional effectiveness:

$$\eta = (T_{aw} - T_m)/(T_f - T_m) \tag{2}$$

The heat fluxes for jet array impingement with an initial crossflow can also be written as in (1), but T_{aw} is now expressed as the non-dimensional adiabatic wall temperature in terms of T_j and T_c (Fig. 6):

$$\eta = (T_{aw} - T_j)/(T_c - T_j) \tag{3}$$

For jet impingement cooling it is appropriate to identify the jet flow as the primary flow and the crossflow as the secondary flow. With this in mind, the form of the definition of η given in (3) for impingement cooling is analogous to the established form utilized for film cooling. However, in the case of impingement it may not be appropriate to refer to this η as an ''effectiveness'' since in cases of practical interest in turbine impingement cooling it is desirable to have the jet flow dominating. This condition is reflected by η approaching zero.

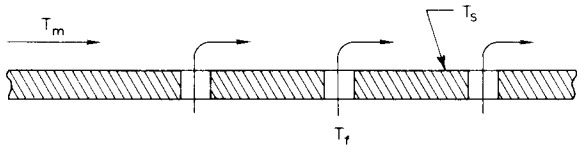

Fig. 5 Film cooling as a three-temperature problem.

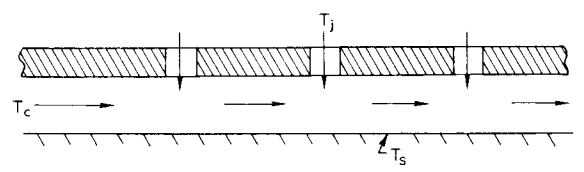

Fig. 6 Jet array impingement with initial crossflow as a three-temperature problem.

It is useful to emphasize that (1) and (3) may be combined to give

$$q = h[(1 - \eta)(T_s - T_j) + \eta\,(T_s - T_c)] \tag{4}$$

This form points up the fact that η is merely a ''temperature-difference weighting factor'', and for jet impingement with crossflow is perhaps best viewed in this manner.

In order to define the heat transfer characteristics (h, η) of a two-dimensional array of discrete impinging jets with an initial crossflow, it is necessary to characterize T_c and T_j. T_c is chosen to characterize the initial crossflow temperature at the entrance to the array portion of the crossflow channel (x = 0, Fig. 3). The entrance location is defined to be one-half a streamwise hole spacing upstream of the first spanwise row of holes in the array. This choice of entrance location is based on the fact that the array heat transfer characteristics (h, η) are considered averaged across the span, but resolved in the streamwise direction to increments x_n, centered immediately opposite each spanwise row of holes. For low-speed flow T_c may be characterized by the mixed-mean temperature of the initial crossflow at the entrance to the array, while T_j may be taken as the mixed-mean fluid temperature at the jet exit plane.

However, for high-speed flow a somewhat generalized definition is necessary, just as in the case of film cooling [13]. T_c may be characterized as the adiabatic wall temperature at the array entrance, and T_j as the adiabatic wall temperature opposite the given jet row in the absence of an initial crossflow. In the case of low-speed flow, these values reduce to the mixed-mean temperatures previously indicated.

In cases of practical interest in turbine cooling the distinction indicated above in establishing T_c and T_j will not be particularly significant since differences between T_s and both T_c and T_j are quite large. However, for the experimental results to be reported herein these temperature differences were small (5 to 35 K). Also with the relatively low laboratory air pressures utilized, jet and crossflow velocity magnitudes in some cases may be rather high. Hence it was appropriate to utilize the more general definition in reducing the heat transfer data obtained from the test runs.

EXPERIMENTAL PROCEDURES AND DATA REDUCTION

Many details of the experimental procedures and data reduction techniques utilized for the initial crossflow tests were similar to or identical with those previously reported in [1]. Those details will be included here only as necessary with emphasis placed primarily on those additional features which were unique to the initial crossflow tests.

Standard Test Runs

A standard test run was initially defined by setting up a selected initial crossflow geometry with x_n/d, y_n/d, and z/d the primary geometric parameters as previously summarized in Table 1. The number of spanwise jet rows was always ten. The centerlines of these rows were always aligned directly opposite the spanwise centerlines of segment numbers 20 through 29 of the test plate, counting from upstream (Fig. 4). Segments 1 through 19 formed the heat transfer surface of the initial crossflow channel, and segments 30 and 31 formed an extension of the heat transfer surface in the exit channel downstream of the array. Values of η and

h, as defined by Eqs. (1) and (3) [or by (4)] were determined for each segment opposite the array (20 through 29) as well as for segment 30 immediately downstream. Segment 31 was used as a guard element. Values of h could also be determined upstream of the array where $\eta = 1$ by definition.

Two separate sets of tests were required to determine these streamwise profiles of η and h for a given geometry, $\overline{Re}_j$, and flow ratio m_c/m_j. First, with the initial crossflow geometry, but with zero initial crossflow ($m_c = 0$), a set of tests was conducted to determine T_j, the characteristic temperature for jet flow alone, for each segment. These tests were conducted at three different steady-state conditions corresponding to three different power input levels to the segment heaters. A linear least squares fit to the three resulting data sets (q, T_s) for each of the segments under the jet rows (plus Segment 30) was used to determine the appropriate T_j for each segment from $q = h(T_s - T_j)$. In addition the fits result in streamwise resolved values of h for the array in the absence of initial crossflow.

Second, a similar set of tests at three different power levels was conducted with the heated initial crossflow present. For the conditions of these tests, the adiabatic wall temperature of the initial crossflow at the entrance to the array, used to characterize T_c, was essentially identical to the mixed-mean stagnation (i.e., total) temperature of the initial crossflow. This stagnation temperature was determined for each steady-state condition from the measured initial crossflow plenum temperature, combined with an energy balance over the initial crossflow channel:

$$T_c = T_o^c + \frac{1}{m_c c_p} \sum_{n=1}^{19} Q_n \qquad (5)$$

With T_j and T_c determined, a linear least squares fit to the three data sets (q, T_s) was used to determine the two unknowns h and η from Eq. (4) for each of the segments 20 through 30. Values of h in the initial crossflow channel were also determined using the adiabatic wall temperature at the given segment as the reference temperature approximated by the local mixed-mean stagnation temperature again determined from an energy balance.

It was shown experimentally by McAdams, et al. [14] that for duct flows at subsonic velocities the heat transfer coefficient defined on the difference between the temperature of the heated wall and adiabatic wall temperature is independent of this difference. They also showed that for such flows preferred values of the recovery factor lie in the range 0.875 to 0.905. Using a recovery factor of 0.89 it was determined that for the present tests the difference between the stagnation temperature and the adiabatic wall temperature for the initial crossflow channel was normally less than 0.1 K, and always less than 0.2K. Hence, the use of the stagnation temperature as satisfactorily representing the adiabatic wall temperature is justified for the conditions of these tests.

Additional details relating to the test procedure will now be discussed. For each standard test run the jet flow rate (m_j) was set at the appropriate value to give a nominal $\overline{Re}_j$ of 10^4. The jet plenum air temperature was normally at an ambient level of about 300K. For each geometry, the initial crossflow rate (m_c) was set, in turn, at the appropriate levels to give nominal values of m_c/m_j of 0.2, 0.5 and 1.0. The initial crossflow plenum air temperature was brought to a value approximately midway between the jet plenum temperature and the maximum value of the heat transfer surface temperature to be utilized (about 330 K).

The first steady-state condition was achieved with zero power input to the test plate segment heaters, and the segment temperatures were recorded. The entire test plate was then brought to a uniform temperature at the maximum value of about 330 K by individually adjusting the power input to each of the 31 test plate segment heaters. When this second steady-state condition was achieved, both the segment temperatures and the individual segment heater power inputs were recorded. The third and final condition was set with the heater power inputs cut to about half of their maximum values. Segment (surface) heat fluxes were determined from the measured power inputs suitably corrected for heat leaks [1]. Heat fluxes for the zero power input condition were not precisely zero because of these small but unavoidable heat leaks.

Test run procedures for the determination of T_j were also as outlined above except for the absence of the initial crossflow. Segments 1 through 18 were inactive with Segment 19 used as a guard element.

Experimental Uncertainties

The linear least squares fit based on Eq. (4) was actually carried out in the form

$$\frac{q}{T_s - T_c} = h(1 - \eta)\frac{T_s - T_j}{T_s - T_c} + h\eta \qquad (6)$$

with the coefficients $h(1 - \eta)$ and $h\eta$ determined directly from the fit. It is clear from either Eq. (4) or (6) that only two independent test conditions are required to determine η and h. The use of three independent conditions provided additional confidence to the fit. As a measure of this confidence three values of η and of h were also computed using each of the three possible combinations of two members of each data set (zero/maximum, zero/half, and half/maximum power input conditions). These values were then compared with the original values of η and h based on the linear least squares fit to all three data sets.

Considering all standard test runs with initial crossflow present, 95% of the values of h computed from two members of each set deviated by less than $\pm$ 3% of the values based on the fit. For η the result was $\pm$ 7% with most of the larger deviations coming at downstream rows where the η values were smaller. The total number of values compared for both η and h was 1188 (12 geometries x 3 initial crossflow rates x 11 segments x 3 values from each three member set). For the zero initial crossflow tests 95% of the h values were within $\pm$ 2%.

The percentage deviations noted above provide some indication of the uncertainty associated with the η and h results. Experimental uncertainties must be at least as large as these values. Composite uncertainties for η and Nu were also calculated by the method of [15]. Input uncertainties were estimated at $\pm$ 1% to $\pm$ 2% for the heat fluxes, $\pm$ 0.25 K for $(T_s - T_c)$, $\pm$ 0.1 K for $(T_s - T_j)$, and $\pm$ 1% for d as it enters the Nusselt number calculated from h. $(T_s - T_j)$ values depended only on differences between measurements made with the same thermocouple, whereas $(T_s - T_c)$ values depended on the difference between measurements from two different thermocouples plus an energy balance. The calculated η and Nu composite uncertainties varied depending on the particular conditions but for Nu within the array most conditions result in values of $\pm$ 6% or less. For η the composite uncertainties, expressed on a percentage basis, vary more widely depending on conditions, from about $\pm$ 2 to $\pm$ 4% for η values near unity to as much as $\pm$ 20% for a downstream value as low as 0.1. Overall,

the calculated composite uncertainty ranges appear consistent with the percentage deviations from the linear least squares fits as summarized in the preceding paragraph.

Special Test Runs

Several special test runs were conducted to examine the sensitivity of the results to changes in certain parameters or conditions normally held constant during the standard test runs. These included the effect of $\overline{Re}_j$, the value of the initial crossflow plenum temperature relative to the jet plenum temperature, and the effect of the thermal entrance length (test surface thermal boundary condition) in the initial crossflow channel upstream of the array. Otherwise the procedures for the special runs were the same as for the standard runs.

With the B(5,8,3)I geometry at m_c/m_j = 0.51 tests were conducted for $\overline{Re}_j = 10^4$ (standard test run value) and also for a larger $\overline{Re}_j$ (1.81 x 10^4). The two resulting streamwise η profiles were found to be independent of jet Reynolds number to within experimental uncertainty. The heat transfer coefficient profiles were plotted as Nusselt numbers normalized by $\overline{Re}_j^{0.73}$ for comparison. The exponent on $\overline{Re}_j$ is from the jet array impingement correlation previously reported [2,11]. This result from the prior correlation accounted quite satisfactorily for the Nusselt number dependence on Reynolds number observed in this test.

With the B(5,4,3)I geometry at m_c/m_j = 0.84 two otherwise identical test runs were conducted, one with the initial crossflow plenum temperature set at a value such that the initial crossflow-to-jet plenum temperature difference was one-third of the maximum surface-to-jet plenum difference, the second with the initial crossflow plenum temperature increased such that the fractional difference was two-thirds. The results for both η and Nu were in agreement to well within experimental uncertainty, providing additional confidence that these coefficients were independent of the temperature differences.

The B(5,4,3)I geometry at m_c/m_j = 0.2 and 1.0, and the B(5,8,3)I geometry at 1.0 were tested with test plate segments 1 through 9 at zero heater power inputs for each of the three steady state conditions comprising a complete test run. This cut the isothermal portion of the entrance length upstream of the array from 15.8 to 8.3 hydraulic diameters (and from 38 to 20 in terms of streamwise hole spacings). The available hydrodynamic entrance length remained constant at 15.8 hydraulic diameters or 38 hole spacings. Again, the results for both η and Nu remained unchanged to well within experimental uncertainty.

RESULTS AND DISCUSSION

Results from the standard test runs for streamwise profiles of η and Nu within the jet array will be presented and discussed shortly. First, however, the heat transfer coefficients in the initial crossflow channel immediately upstream of the jet array section will be considered and compared with prior data from the literature.

For all standard test runs reported here the entrance length and the width (span) of the initial crossflow channel were fixed, as was the width of the heat transfer test plate (Table 1). The entrance length (Le) measured in terms of hydraulic diameters (D_h = 2z) varied with the channel height z set for the particular test. Measured to the center of Segment 19, the first segment upstream of the jet array, L_e/D_h ranged from 15.4 to 92.5. The aspect ratio of the channel cross-section also varied with z, and ranged from 24 to 144. The corresponding aspect ratio of the cross-section reckoned with respect to the width of the test plate varied from 16 to 96. Hence, both hydrodynamic and heat transfer edge effects could be considered negligible; and the configuration closely approximated an infinite parallel plate duct with asymmetric heating such that the primary heat transfer surface was isothermal while the opposing surface was essentially adiabatic. Some prior measurements for heat transfer with turbulent flow under similar conditions are available in the literature [16,17]. For the present test, initial crossflow channel Reynolds numbers (Re_c) ranged from 4 x 10^3 to 4 x 10^4. Nominal values of Re_c (~ 10^4 and 2 x 10^4) for a number of test runs were nearly the same as the values at the ends of the range covered by Tan and Charters [17], 9.5 x 10^3 to 2.12 x 10^4. Their test results, which included the entrance length, were for a 4.75 cm high rectangular duct with an aspect ratio of 3 with one large side heated. Nusselt number values for the present tests were adjusted according to $Re_c^{0.8}$ in order to compare directly to the Tan and Charters' data. Channel Nusselt numbers (hD_h/k) at Segment 19 from the present tests are compared with their results in Fig. 7. The two sets of results are seen to be quite consistent. A fully developed Nusselt number magnitude based on the data of Sparrow, et al. [16] for a 5:1 aspect ratio duct heated on one large side only shown in Fig. 7 is also seen to be quite consistent. The data point utilized from Sparrow, et al. was at Re_c = 1.85 x 10^4 with the Nusselt number also adjusted according to $Re_c^{0.8}$ for direct comparison in Fig. 7.

We turn now to the results for heat transfer characteristics in the jet array impingement region with the presence of the initial crossflow at a temperature different from the jet temperature. Sample results drawn from the standard test series are presented for four different geometric configurations in Figs. 8 through 10. Each figure shows streamwise profiles of η and Nu resolved to one streamwise hole spacing. η and Nu are paired in each figure to emphasize that, in general, in order to appropriately relate the heat flux to the surface and characteristic fluid temperatures both parameter values are needed. For each geometry profiles are shown for m_c/m_j at nominal values of 0.2, 0.5, and 1.0. Nusselt number profiles for the initial crossflow configuration, but with m_c = 0, are also

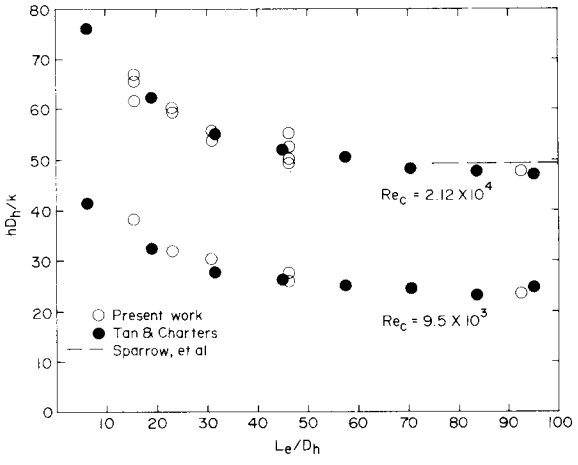

Fig. 7 Nusselt numbers in initial crossflow channel at entrance to jet array compared with prior data from literature.

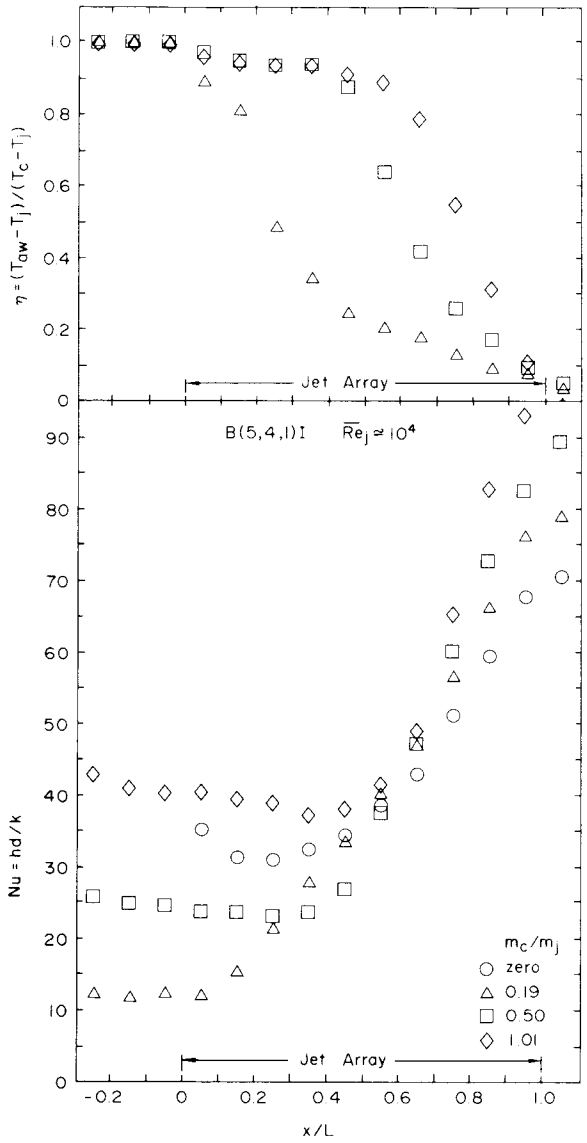

Fig. 8 Effect of initial crossflow rate on η and Nu profiles for B(5,4,1)I geometry.

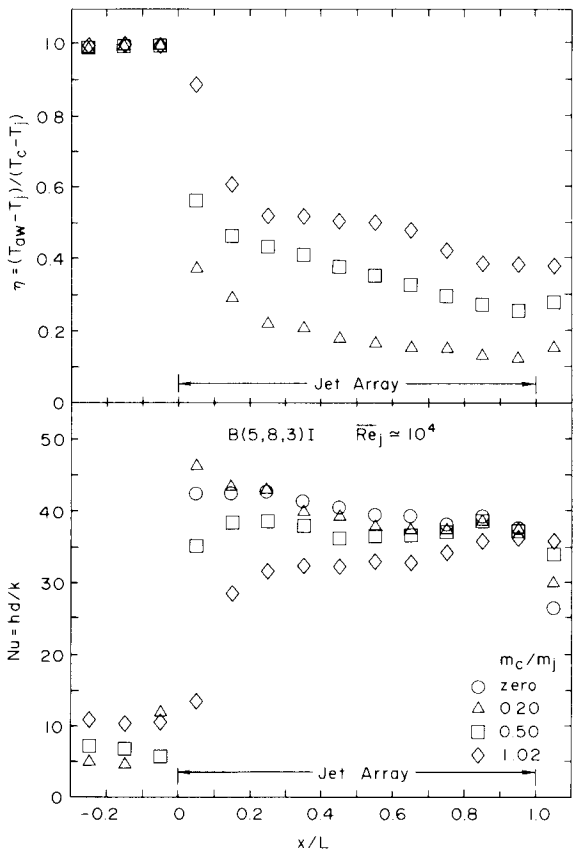

Fig. 9 Effect of initial crossflow rate on η and Nu profiles for B(5,8,3)I geometry.

shown as a reference or baseline case for comparison. Since each array had ten spanwise rows of holes, each profile includes ten points within the array proper, with three additional points included for the initial crossflow channel immediately upstream of the array and one point immediately downstream.

Examine first the values of η. In general, η decreases with increasing x/L and decreasing m_c/m_j. These trends simply reflect the increasing influence of the jet flow. It may be emphasized that since the crossflow temperature was characterized by its value at the entrance to the array, the value of η at a specific row reflects the influence of the jet flow introduced at every upstream row as well as that of the row in question. Of particular note is the fact that overall, η covers the range from unity to nearly zero, and for the B(5,4,1)I geometry represented by Fig. 8, covers this range for a single configuration. This geometry also has the most highly nonuniform flow distribution (Fig. 11). Note that here the effect of initial crossflow not only penetrates into the array, but essentially dominates ($\eta \simeq 1$) at the first row for all m_c/m_j; and for $m_c/m_j = 0.5$ and 1.0, dominates over halfway through the array. This dominance can also be seen by examining the Nu profiles for this case which remain essentially at their upstream initial crossflow channel levels well into the array. This behavior is quite consistent with the very large cross-to-jet mass velocity ratios which were observed to persist well into this array (Fig. 11).

Turning to Fig. 9 a contrasting behavior is observed for the geometry with the most nearly uniform flow distribution (Fig. 12). Here η has already dropped to about one-half at the first row, except for $m_c/m_j = 1.0$, where this occurs at the second row. Similarly, the strong immediate influence of the jets is reflected in the very large increase in Nu from immediately upstream of the array to the very first row of jets (excepting the $m_c/m_j = 1.0$ case in which the change is again less pronounced). It is interesting to note that at the first row an increase of G_c/G_j (Fig. 12) from 0.2 to 0.4 causes a reduction in Nu (Fig. 9) by a factor of more than two-and-one-half, while the increase from 0 to 0.2 causes essentially no change. It is possible that at the larger value of G_c/G_j the impingement points of the jets are displaced downstream by $x_n/2$ or more and thus provide little cooling of the area $0 \leq x \leq x_n$ associated with the first row. This explanation is reinforced by examining the Nu values immediately downstream of the array. For $m_c/m_j = 1.0$ this Nu value is 3.5 times the value upstream of the array though the downstream crossflow Reynolds number

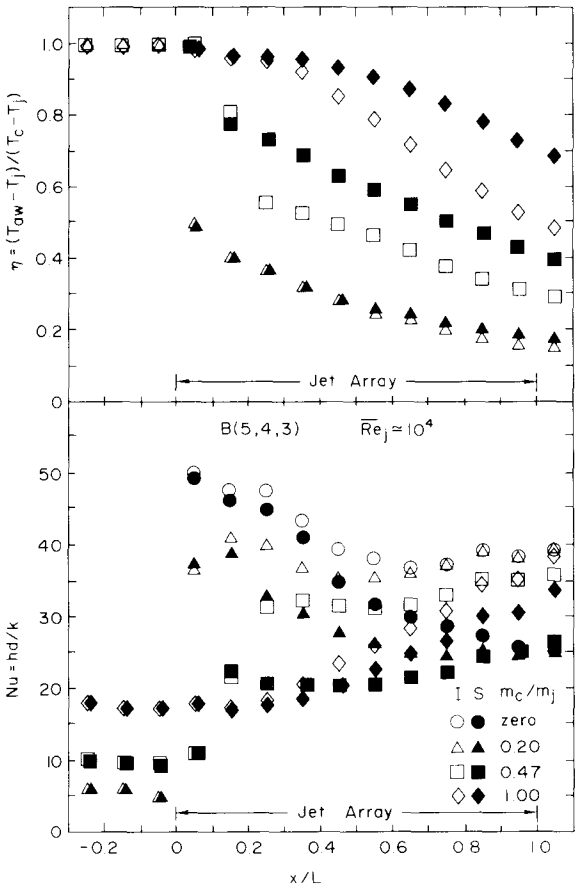

Fig. 10 Effect of initial crossflow rate on η and Nu profiles for B(5,4,3) geometry. I = inline pattern, S = staggered pattern.

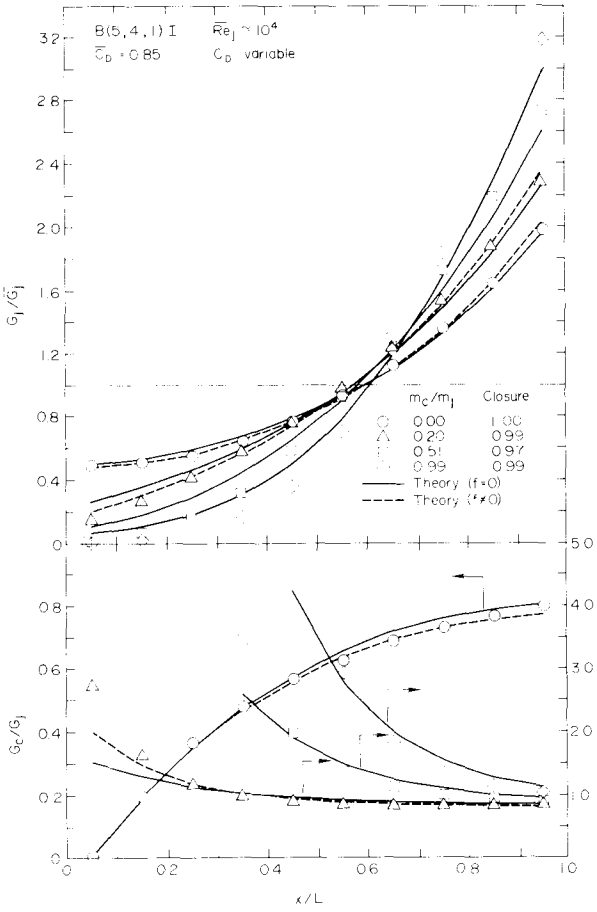

Fig. 11 Effect of initial crossflow on jet array flow distribution for B(5,4,1)I geometry - experimental data compared with predictive model [12].

would be just twice that upstream of the array. This indicates that the jets in the last row of the array must be displaced enough to be impinging on the surface segment immediately downstream of the array.

The final sample results for η and Nu presented here (Fig. 10) are for the B(5,4,3) geometry, for both inline and staggered hole patterns. The flow distributions for this geometry (not shown here) fall between those for the two inline geometries of Figs. 8 and 9. Considering the relative flow distributions the results for the inline pattern in Fig. 10 are consistent with the trends exhibited for η and Nu in Figs. 8 and 9 as discussed in the preceding paragraphs. The results for the staggered hole pattern included in Fig. 10 will be discussed shortly. Complete graphical and tabular results for both heat transfer characteristics and flow distributions for all geometries tested (Table 1) may be found in [18].

Considering the entire set of results, the Nu profiles, unlike the η profiles, do not all vary monotonically with streamwise location. Rather, Nu variations include monotone decreasing, monotone increasing, and cases with one or two local minima and/or maxima. An important observation to emphasize is that in most cases the addition of the initial crossflow (which means an increase in the total coolant flow, since m_j was kept essentially constant for each geometry), resulted in reduced mean values of Nusselt number over the jet array region. Of all the arrays tested only those with z/d = 1 showed higher mean values of Nu at one or more of the initial crossflow values, as compared with the zero initial crossflow case. Even these cases resulted in a degradation in mean Nusselt number due to the presence of an initial crossflow, when considered per unit of total coolant flow rate ($m_c + m_j$).

Finally, consider the results for the staggered array, B(5,4,3)S as compared with the results for its inline counterpart in Fig. 10. This geometry was selected for testing with a staggered hole pattern since in prior noninitial crossflow tests it showed the largest effect of hole pattern on the spanwise averaged heat transfer coefficients [1,8]. It has the closest hole spacings and largest z/d of all the arrays tested. Streamwise flow distributions for this staggered pattern were found to be essentially the same as those for the inline case. The η profiles for the staggered array fall above those for the inline array, insignificantly for the smallest initial crossflow ratio, m_c/m_j = 0.2, but noticeably for m_c/m_j = 0.5 and 1.0, especially downstream.

For all flow ratios from zero to unity, the staggered array Nusselt numbers are the same as the inline values at the first upstream row in the array with inline values becoming larger than the staggered values as one proceeds downstream. An explanation for this type of behavior was originally presented in some detail in connection with noninitial crossflow test

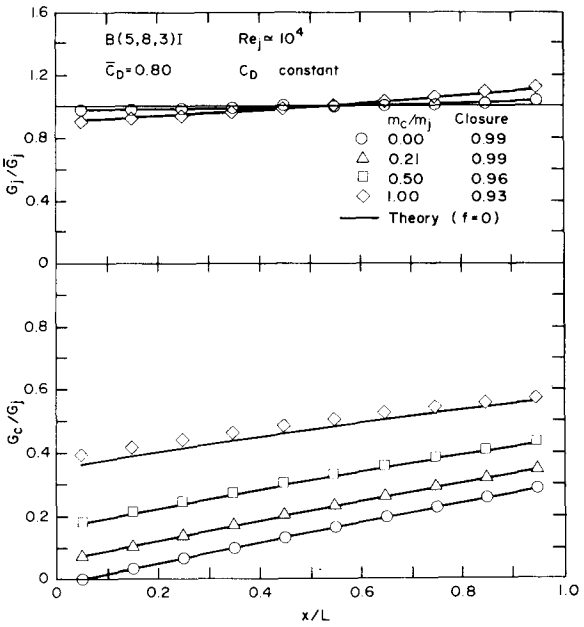

Fig. 12 Effect of initial crossflow on jet array flow distribution for B(5,8,3)I geometry - experimental data compared with predictive model [12].

results [1,9]. Basically it may be speculated that there is less mixing of the jet and crossflow at downstream rows for the inline pattern than for the staggered pattern. Hence, the inline impinging jets more nearly retain their identity and provide more effective cooling than those in the staggered pattern. Though the phenomena involved is extremely complex, so that conclusive explanations are premature, the η behavior also fits the above intepretation in that the jets are less dominant in the staggered case since they mix somewhat more with the crossflow.

Prior heat transfer measurements for one geometric configuration for a two-dimensional array of circular impinging jets with an initial crossflow were made by Saad, et al. [10]. Only Nusselt number results were presented. No indication of adiabatic wall temperatures or the relation of the initial crossflow temperatures to the jet temperatures was given. The Nusselt numbers could not be directly compared with results of the present measurements, because the hole spacings of the array studied in [10] were below the range covered in the present study. However, on a relative basis, the Nusselt number magnitudes were consistent with the present results.

CONCLUDING REMARKS

Experimentally determined spanwise averaged, streamwise resolved dimensionless adiabatic wall temperatures (η values) and Nusselt numbers for jet arrays with ten spanwise rows of holes in the presence of an initial crossflow have been presented. The η values within the array, under some conditions, span the range from unity to nearly zero. Nusselt numbers at the upstream rows of the array are in many cases significantly reduced even by small initial crossflow rates relative to the total jet flow rate. The practical implication of these results is of considerable importance. For example, in a highly cooled first stage vane like that shown in Fig. 1, T_c is often several hundred degrees above T_j. Typical values are T_s = 1260 K, T_j = 760 K, and T_c = 870 K. The present results for η and Nu, if converted to heat fluxes, imply that local cooling rate predictions within the array could, in many cases, easily be in error by 100% or more depending on the designer's guess, in the event he did not have available to him detailed quantitative results for the effect of the initial crossflow rate and temperature. There is evidence that unacceptable levels of design uncertainty exist in practice, and that premature failures of impingement cooled airfoils have been the result. With better information available on the effects of initial crossflow, it should be possible to make significant improvements in design and to further develop the full potential of impingement cooled gas turbine vanes and blades. The designer's need for appropriate information on η may be further emphasized by observing that even with appropriate values available for h, given the heat flux and values for T_c and T_j, predictions for T_s will differ by an amount equivalent to $T_c - T_j$ (110 K for the above example) as η is varied from unity to zero.

It should be emphasized that the η values presented, though resolved in the streamwise direction, are defined in terms of the initial crossflow temperature at the entrance to the array. In applications of these coefficients, the designer should also use this characteristic temperature. As a good approximation the stagnation temperature (mixed-mean value) at the entrance to the array may be used. Or, for better accuracy, the corresponding adiabatic wall temperature may be used, computed on the basis of a recovery factor. Unless more specific information is available for the particular conditions being considered, a recovery factor of 0.9 is recommended [14].

Most of the measurements were carried out for nominal mean jet Reynolds number values of 10^4. The Nusselt number data tabulated in Appendix D, Table D.2 of [18] may be applied at other $\overline{Re}_j$ (or Re_j) by assuming the Nusselt numbers to be proportional to $Re_j^{0.73}$ [2,11], unless upstream rows are being considered in a case where the initial crossflow dominates ($\eta \sim 1$). Then, the use of the exponent 0.80 on the Reynolds number is recommended since a duct or channel-like flow is not only penetrating within the array but dominating the flow field.

ACKNOWLEDGMENT

The support of the National Aeronautics and Space Administration, Lewis Research Center, under Grant NSG 3075 is hereby gratefully acknowledged.

REFERENCES

1. Florschuetz, L.W., Metzger, D.E., Takeuchi, D.I. and Berry, R. A., Multiple Jet Impingement Heat Transfer Characteristic - Experimental Investigation of Inline and Staggered Arrays with Crossflow, NASA Contractor Report 3217, Department of Mechanical Engineering, Arizona State University, Tempe, January 1980.

2. Florschuetz, L.W., Metzger, D.E. and Truman, C.R., Jet Array Impingement with Crossflow--Correlation of Streamwise Resolved Flow and Heat Transfer Distributions, NASA Contractor Report 3373, Department of Mechanical Engineering, Arizona State University, Tempe, January 1981.

3. Kercher, D.M. and Tabakoff, W., ''Heat Transfer by a Square Array of Round Air Jets Impinging Perpendicular to a Flat Surface Including the Effect of Spent Air,'' ASME Journal of Engineering for Power, Vol. 92, No. 1, Jan. 1970, pp. 73-82.

4. Hollworth, B.R. and Berry, R.D., ''Heat Transfer from Arrays of Impinging Jets with Large Jet-to-Jet Spacing,'' ASME Journal of Heat Transfer, Vol. 100, 1978, pp. 352-357.

5. Gauntner, J.W., Gladden, H.J., Gauntner, D.J. and Yeh, F.C., ''Crossflow Effects on Impingement Cooling of a Turbine Vane,'' NASA TM X-3029, March 1974.

6. Bouchez, J.P. and Goldstein, R.J., ''Impingement cooling From a Circular Jet in a Crossflow,'' International Journal of Heat and Mass Transfer, Vol. 18, 1975, pp. 719-730.

7. Sparrow, E.M., Goldstein, R.J. and Rouf, M.A., ''Effect of Nozzle-Surface Separation Distance on Impingement Heat Transfer for a Jet in a Crossflow,'' ASME Journal of Heat Transfer, Vol. 97, 1975, pp. 528-533.

8. Metzger, D.E., Florschuetz, L.W., Takeuchi, D.I., Behee, R.D. and Berry, R.A., ''Heat Transfer Characteristics for Inline and Staggered Arrays of Circular Jets with Crossflow of Spent Air,'' ASME Journal of Heat Transfer, Vol. 101, 1979, pp. 526-531.

9. Florschuetz, L.W., Berry R.A. and Metzger, D.E., ''Periodic Streamwise Variations of Heat Transfer Coefficients for Inline and Staggered Arrays of Circular Jets with Crossflow of Spent Air,'' ASME Journal of Heat Transfer, Vol. 102, 1980, pp. 132-137.

10. Saad, N.R., Mujumdar, A.S., Abdel Messeh, W. and Douglas, W.J.M., ''Local Heat Transfer Characteristics for Staggered Arrays of Circular Impinging Jets with Crossflow of Spent Air,'' ASME Paper 80-HT-23, 1980.

11. Florschuetz, L.W., Truman C.R. and Metzger, D.E., ''Streamwise Flow and Heat Transfer Distributions for Jet Array Impingement with Crossflow ,'' ASME Journal of Heat Transfer, Vol. 103, 1981, pp. 337-342.

12. Florschuetz, L.W. and Isoda, Y., ''Flow Distributions and Discharge Coefficient Effects for Jet Array Impingement with Initial Crossflow,'' ASME Paper 82-GT-156, 27th International Gas Turbine Conference, London, April 1982 (in press, Journal of Engineering for Power).

13. Goldstein, R.J., ''Film Cooling,'' Advances in Heat Transfer, Vol. 7, 1971, pp. 321-379.

14. McAdams, W.H., Nocolai, A.L. and Keenan, J.H., ''Measurements of Recovery Factors and Coefficients of Heat Transfer in a Tube for Subsonic Flow of Air,'' Transactions AIChE, Vol. 42, 1946, pp. 907-925.

15. Kline, S.J. and McClintock, F., ''Describing Uncertainties in Single Sample Experiments,'' Mechanical Engineering, Vol. 75, January 1953, pp. 3-8.

16. Sparrow, E.M., Lloyd, J.R. and Hixon, C.W., ''Experiments on Turbulent Heat Transfer in an Asymmetrically Heated Rectangular Duct,'' ASME Journal of Heat Transfer, Vol. 88, 1966, pp. 170-174.

17. Tan, H.M. and Charters, W.W.S., ''An Experimental Investigation of Forced-Convective Heat Transfer for Fully-Developed Turbulent Flow in a Rectangular Duct with Asymmetric Heating,'' Solar Energy, Vol. 13, 1970, pp. 121-125.

18. Florschuetz, L.W., Metzger, D.E., Su, C.C., Isoda, Y. and Tseng, H.H., Jet Array Impingement Flow Distributions and Heat Transfer Characteristics - Effects of Initial Crossflow and Nonuniform Array Geometry, NASA Contractor Report 3630, Department of Mechanical and Aerospace Engineering, Arizona State University, Tempe.